Polar Magnetic Oxides

DOI: 10.1002/anie.201302775

Polar and Magnetic Mn_2FeMO_6 (M = Nb, Ta) with $LiNbO_3$-type Structure: High-Pressure Synthesis**

*Man-Rong Li, David Walker, Maria Retuerto, Tapati Sarkar, Joke Hadermann, Peter W. Stephens, Mark Croft, Alexander Ignatov, Christoph P. Grams, Joachim Hemberger, Israel Nowik, P. Shiv Halasyamani, T. Thao Tran, Swarnakamal Mukherjee, Tanusri Saha Dasgupta, and Martha Greenblatt**

Polar oxides are of much interest in materials science and engineering. Their symmetry-dependent properties, such as ferroelectricity/multiferroics, piezoelectricity, pyroelectricity, and second-order harmonic generation (SHG) effect are important for technological applications.[1] However, polar crystal design and synthesis is challenging, because multiple effects, such as steric or dipole–dipole interactions, typically combine to form non-polar structures; thus the number of known polar materials, especially polar magnetoelectric materials, is still severely restricted.[2] Therefore, it is necessary for the material science community to develop new strategies to create these materials.

Recently, exotic ABO_3-type perovskites with unusually small A-site cations have attracted much attention owing to the formation of $LiNbO_3$ (LN)-type polar structure at high pressure (HP; Supporting Information, Section S1).[3] So far, several LN-type ABO_3 oxides have been discovered as metastable quenched phases, including $ZnSnO_3$,[4a] $CdPbO_3$,[4b] $(In_{1-x}\square_x)MO_{3-\delta}$ (M = Mn/Fe, $\square$ = vacancy),[5] $ScFeO_3$,[3b] and the high-pressure polymorphs of $MnMO_3$ (M = Ti, Sn)[6] and $FeTiO_3$,[7] which show either SHG[4] or (near) room-temperature (RT) multiferroic behavior.[3,5–7] Compared with the research in HP-stabilized LN-type ABO_3 oxides, there are few studies of systems with multiple B-site cations, such as $A_2BB'O_6$, containing small A-ions. Occupation of the octahedral B sublattice by two or more different cations can generate interesting physical properties, such as magnetoresistance.[8] To the best of our knowledge, to date, only Mn_2BSbO_6 (B = Fe, V, Cr, Ga, Al) with a small A (Mn^{2+}) and mixed B-site cations have been stabilized under HP.[9,10] Among the Mn_2BSbO_6 HP phases, Mn_2FeSbO_6 is potentially the most interesting, as it displays a sharp magnetic transition around 270 K, which is due to the magnetic interactions of $Mn^{+2}(d^5)$ and Fe^{+3} (d^5); however, it adopts a hexagonal centrosymmetric ilmenite (IL) structure. Herein, we present the synthesis of polar LN-type magnetic oxides Mn_2FeMO_6 (M = Nb, Ta) in the $A_2BB'O_6$ family, and investigate their crystal structures, formal oxidation states, magnetic properties, SHG effect, and dielectric properties. Theoretical calculations within the framework of density functional theory (DFT) supplemented with Coulomb interaction, *U*, were also carried out to provide theoretical verification of the experimental results.

Mn_2FeMO_6 (M = Nb, Ta) were prepared at 1573 K under 7 GPa in a Walker-type multianvil press (details of the synthesis are presented in the Supporting Information, Section S2).[11] The powder synchrotron X-ray diffraction (SXRD) patterns of the as-prepared Mn_2FeMO_6 (Figure 1) could be indexed to rhombohedral unit cells ($a \approx 5.27$ Å, $c \approx 13.9$ Å), and Rietveld refinement quickly showed the LN

[*] Dr. M. R. Li, M. Retuerto, T. Sarkar, M. Greenblatt
Department of Chemistry and Chemical Biology, Rutgers
The State University of New Jersey
610 Taylor Road, Piscataway, NJ 08854 (USA)
E-mail: martha@rutchem.rutgers.edu
Dr. D. Walker
Lamont-Doherty Earth Observatory, Columbia University
61 Route 9W-PO Box 1000, Palisades, NY 10964 (USA)
Dr. J. Hadermann
EMAT, University of Antwerp
Groenenborgerlaan 171, 2020 Antwerp (Belgium)
Dr. P. W. Stephens
Department of Physics & Astronomy State University of New York
Stony Brook, NY 11794 (USA)
Dr. M. Croft, A. Ignatov
Department of Physics & Astronomy, Rutgers
The State University of New Jersey
136 Frelinghuysen Road, Piscataway, NJ 08854 (USA)
Dr. C. P. Grams, J. Hemberger
II. Physikalisches Institut, Universität zu Köln
50937 Köln (Germany)
Dr. I. Nowik
Racah Institute of Physics, Hebrew University
Jerusalem, 91904 (Israel)
Dr. P. S. Halasyamani, T. T. Tran
Department of Chemistry, University of Houston
136 Fleming Building, Houston, TX 77204 (USA)
Dr. S. Mukherjee, Dr. T. S. Dasgupta
Department of Condensed Matter Physics and Materials Sciences
S. N. Bose National Centre for Basic Sciences
JD Block, Sector III, Salt Late, Kolkata 700098 (India)

[**] This work was supported by the NSF-DMR-0966829 grant, Rutgers University (Board of Governor Prof. Grant), and the DOD-VV911NF-12-1-0172 grant. Use of the National Synchrotron Light Source, Brookhaven National Laboratory was supported by the DOE BES (DE-AC02-98CH10886). P.S.H. and T.T.T. thank the Welch Foundation (Grant E-1457) for support.

Supporting information for this article is available on the WWW under http://dx.doi.org/10.1002/anie.201302775.

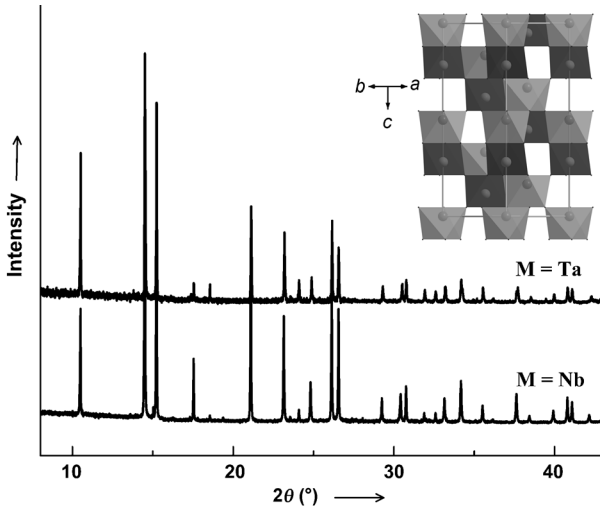

Figure 1. Powder SXRD patterns of Mn_2FeMO_6 (M = Nb (bottom) and Ta (top)). $\lambda = 0.6997$ Å. Inset: the LN-type unit-cell crystal structure of Mn_2FeMO_6, where Mn is located at the A site and Fe/M are disordered over the B site. MnO_6 octahedra gray, $(Fe/M)O_6$ octahedra black.

structure type. It is important to confirm the polar space group; therefore, convergent-beam electron diffraction (CBED) and selected-area electron diffraction (SAED; Supporting Information, Section S3) were used to determine the presence ($R\bar{3}c$) or absence ($R3c$) of an inversion center.[12] CBED patterns and tilt series of SAED patterns taken from Mn_2FeNbO_6 are shown at the bottom and top of Figure 2,

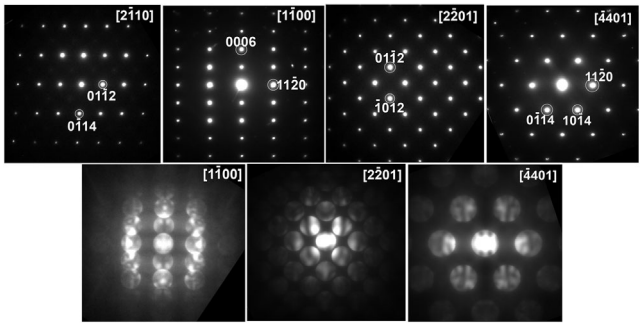

Figure 2. SAED (top) and CBED (bottom) of Mn_2FeNbO_6, showing the polar nature of the hexagonal cell.

respectively. These electron-diffraction patterns could be completely indexed with the cell parameters from the XRD refinements. The reflection conditions derived from the patterns are: $hkil$: $-h+k+l=3n$, $h-h0l$: $h+l=3n$ and $l=2n$ and $000l$: $l=6n$. The $000l$: $l=6n+3$ reflections that are observed on the $[1\bar{1}00]$ are due to double diffraction, as is confirmed by the appearance of Gjonnes–Moodie lines through these reflections on the corresponding CBED pattern. Some of the $[2\bar{1}\bar{1}0]$ zones show very weak sharp and some show weak diffuse reflections at $000l$: $l=6n+3$ and $h\bar{h}0l$: $l=2n+1$, violating these reflection conditions. This can be due to the presence of local order. The trigonal extinction symbols matching these reflection conditions are $R(\mathrm{obv})--$ and $R(\mathrm{obv})-c$. The $[u-u.w]$ zones $[1\bar{1}00]$, $[2\bar{2}01]$, and $[\bar{4}401]$ show as whole pattern symmetry m. Within the trigonal point groups, this whole pattern symmetry corresponds to point groups 32 and $3m$. Combining the information from CBED and SAED leaves only the space group $R3c$ as a possibility, in agreement with the SXRD results. Further observation of positive SHG effect also confirms the non-centrosymmetric character of the structure of both materials (Supporting Information, Section S5).

Subsequent Rietveld refinements of the SXRD data are given in the Supporting Information, Section S4 (Figure S3a, S3b; Tables S1 and S2). The inset of Figure 1 shows a polyhedral view of the unit cell of Mn_2FeMO_6 (M = Nb, and Ta) with a typical LN-type structure, where Mn occupies a six coordinated A site to form MnO_6 octahedra, and Fe and M are disordered on the six coordinated B site in $(Fe/M)O_6$ octahedra. MnO_6 and $(Fe/M)O_6$ groups are arranged to avoid edge-sharing between homonuclear octahedra; the heteronuclear edge-shared octahedra, forming $[Mn(Fe/M)]O_{10}$ dimers, are arranged to form three-dimensional connectivity by face-sharing between the octahedral layers (Supporting Information, Figure S1). The average ⟨Mn-O⟩ bond lengths are 2.16(1) and 2.22(2) Å for M = Nb and Ta, respectively and are comparable with the average ⟨Mn-O⟩ distance of MnO_6 octahedron in $Mn^{2+}Ti^{4+}O_3$ (2.199 Å)[13] and $Mn^{2+}{}_2Fe^{3+}Sb^{5+}O_6$ (2.173 Å),[9] but longer than those in $LaMn^{3+}O_3$ (2.020 Å)[14] and $YMn^{3+}O_3$ (2.036 Å),[14] which is consistent with the expected formal oxidation state of Mn^{+2} in Mn_2FeMO_6. The metal–oxygen distances in the $(Fe/M)O_6$ octahedra are 2.030(6) (M = Nb) and 2.012(20) Å (M = Ta), comparable to ⟨Fe/M-O⟩ of disordered B site perovskites, such as $Sr_2Fe^{3+}M^{5+}O_6$ (1.996 Å for M = Nb,[15] 1.992 Å for M = Ta[16]), and $Pb_2Fe^{3+}M^{5+}O_6$ (2.005 Å for M = Nb[17] and Ta[18]). Thus, the crystal structure analysis indicates a cation formal oxidation state of $Mn^{2+}{}_2Fe^{3+}M^{5+}O_6$, which is further confirmed by X-ray absorption near-edge spectroscopy (XANES) studies (Supporting Information, Section S6).

The magnetic properties of Mn_2FeMO_6 (M = Nb, Ta) show reproducible behavior for samples from different HP batches. Figure 3 shows the evolution of χ_{dc} versus temper-

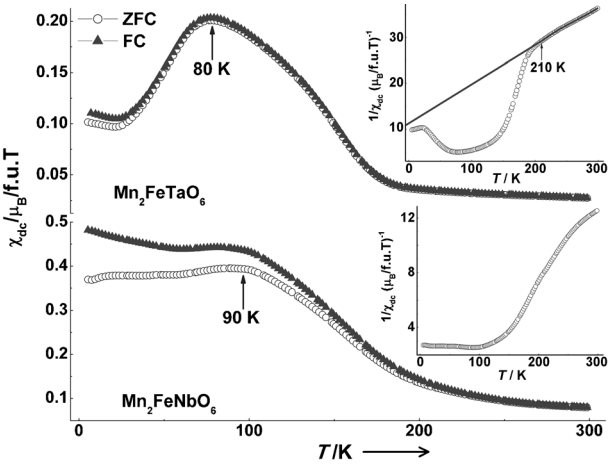

Figure 3. χ_{dc} vs temperature for Mn_2FeTaO_6 (top) and Mn_2FeNbO_6 (bottom) recorded in the ZFC as well as FC modes. Insets: the $1/\chi_{dc}$ versus T plots. f.u.T = formula unit Tesla.

ature for Mn_2FeTaO_6 (top) and Mn_2FeNbO_6 (bottom) samples recorded in zero-field cooled (ZFC) and field cooled (FC) modes. A clear difference in the behavior of the Nb and Ta samples is evident. For Mn_2FeTaO_6 (Figure 3 top), χ_{dc} shows a relatively sharp increase as the oxide is cooled below 200 K, indicating the emergence of magnetic order at this temperature. Below about 80 K, the magnetization starts falling rapidly. Note that this sharp drop is seen in both the ZFC and FC modes, thereby indicating a transition to a strong antiferromagnetic (AFM) state. The Mn_2FeNbO_6 sample, on the other hand, does not exhibit such sharp transitions (Figure 3 bottom). The emergence of magnetic order below 200 K is more gradual here. This is also clearly seen in the $1/\chi_{dc}$ vs T plots (insets of Figure 3), while the paramagnetic region above 200 K in Mn_2FeTaO_6 follows the Curie–Weiss behavior (as evidenced by the linearity of the plot at $T>$ 200 K), this is not the case for Mn_2FeNbO_6, where the $1/\chi_{dc}$ plot is not linear even for $T>200$ K. In fact, the non-linearity extends well up to $T=300$ K, which indicates the presence of residual magnetic interactions even at RT. Below about 90 K, there is a slight drop in the susceptibility of Mn_2FeNbO_6, both in the ZFC and FC curves, but in this case with a divergence between them, which indicate a transition to an AFM state with magnetic frustrations in the system. The high-temperature inverse susceptibility data for the Mn_2FeTaO_6 sample could be fitted to a Curie–Weiss law, $\chi = C/(T-\theta_{CW})$. The fitting allowed us to extract the effective magnetic moment (μ_{eff}) = 10.07 μ_B, which agrees well with the calculated spin only moment per formula unit, $\mu_{calc}=10.25\ \mu_B$; for $\mu_{Mn^{2+}} = \mu_{Fe^{3+}} = 5.92\ \mu_B$. The Curie–Weiss constant, obtained from the fitting, $\theta_{CW}=-165$ K consistent with the presence of AFM interactions.

In Figure 4a (top), we show the isothermal M versus H curves of Mn_2FeTaO_6 recorded at various temperatures in the range 5–300 K. The inset of Figure 4a (top) shows an expanded view near the origin. For $T>200$ K, M versus H is perfectly linear with the curves passing through the origin. These curves correspond to the sample in the paramagnetic region. For $T<200$ K, a small S-shaped hysteresis loop opens up near the origin. This is probably a manifestation of the emergence of canted ferromagnetism. It is important to note that the M–H curves show no sign of saturation for an applied magnetic field as high as $H=5$ T, indicating that the FM interactions are very weak, which is possibly due to spin canting. Below the AFM transition at $T\approx 80$ K, this S-shaped hysteresis loop vanishes, indicating a complete transition to the AFM state. The isothermal M–H curves of Mn_2FeNbO_6 (Figure 4a (bottom)) reveal a different behavior. The S-shaped hysteresis loop is present in this sample down to the lowest temperature measured ($T=5$ K), which indicates that FM interactions, again possibly due to spin canting, are present even at low temperatures. Furthermore, even at the highest measured temperature ($T=300$ K), the M–H curve is not perfectly linear (inset of Figure 4a (bottom)), thereby showing that the sample does not reach a pure paramagnetic state even at RT.

The magnetic nature of Mn_2FeMO_6 is further confirmed by Mössbauer spectra (Supporting Information, Section S7). Figure 4b shows the Mössbauer spectra of Mn_2FeNbO_6,

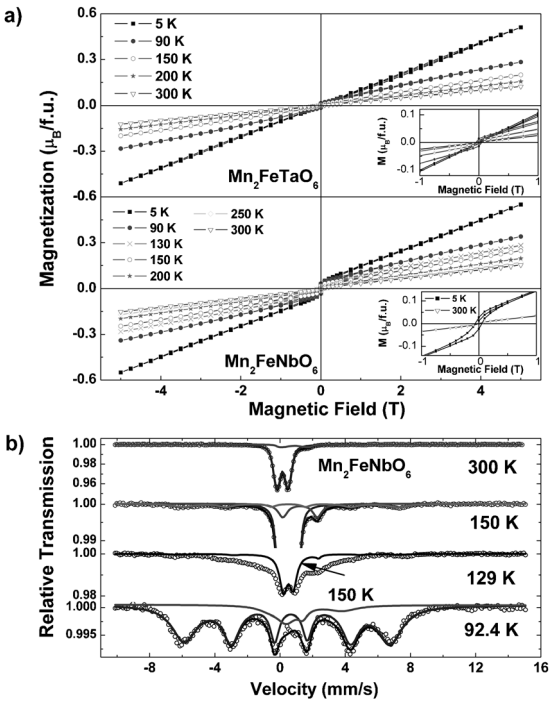

Figure 4. *M* versus *H* curves for a) Mn_2FeTaO_6 (top) and Mn_2FeNbO_6 (bottom); b) Mössbauer spectra of Mn_2FeNbO_6 between 90 and 300 K.

where the beginning of the appearance of the sextet at 150 K is observed, which suggests that the sample is at least partially ordered at this temperature. At 92 K the sextet is clearly resolved, consistent with a complete magnetic ordering. The data on Mn_2FeTaO_6 show similar behavior. Thus, we can conclude that the magnetic ordering temperatures in both samples are between 200 and 250 K. The Mössbauer study also provides information about the oxidation state and the positions occupied by Fe cations. Analysis of the data shows that about 92% of iron is trivalent, in good agreement with the XANES results. It also shows the existence of divalent iron (ca. 8%), which is probably due to cation exchange between Mn and Fe in both A and B sites and/or oxygen defects, which cannot be distinguished by X-ray and electron diffraction studies, since the very similar X-ray scattering factors of Mn ($Z=25$) and Fe ($Z=26$) prevent unambiguous determination of the extent of ordering.

DFT + U calculations[19] (Supporting Information, Section S8) indicate that both compounds have finite polarization owing to the presence of d^0 ions Nb^{+5} and Ta^{5+}, while the magnetism arises owing to presence of Mn and Fe. Figure 5 shows the exchange interaction between Mn and Fe to be of AFM nature. The magnetic lattice connecting Mn and Fe atoms consist of triangular arrangements, which renders the AFM interaction frustrated. Such frustration may give rise to non-collinearity of spins. Our non collinear calculations gave rise to solution with canted magnetization axis of Mn and Fe spins and a small uncompensated net moment. The calculated noncollinear arrangement of spins may be checked by further experiments. The nominal d^5 valences of Mn and Fe, and d^0 valences of Nb and Ta, have also been confirmed through spin-polarized DFT + U calculations, which gave rise to

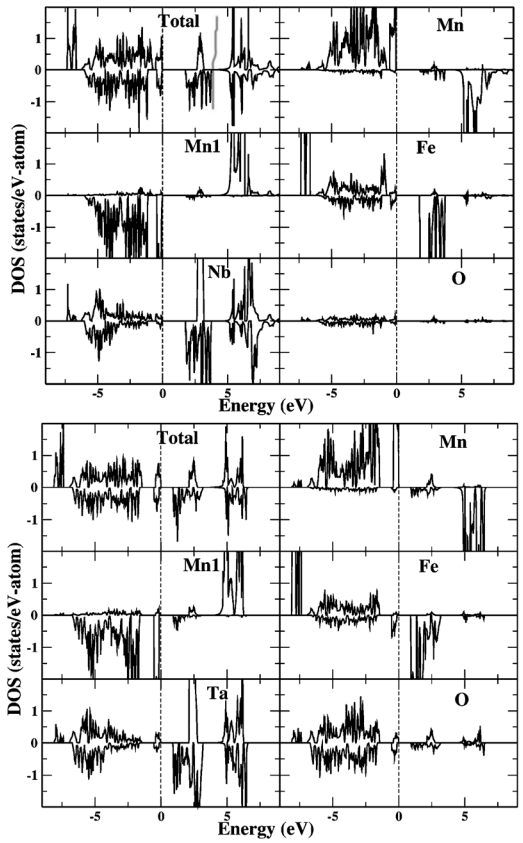

Figure 5. Total and Mn d, Mn1 d, Fe d, Nb/Ta d, and O p projected density of states (DOS) for Mn_2FeNbO_6 (top) and Mn_2FeTaO_6 compounds (bottom), as calculated in GGA + U approximation. The zero of the energy is fixed at the calculated Fermi energies.

calculated spin magnetic moments of about 4.2–4.5 μ_B at Mn and Fe sites, in conformity with high spin 2 + and 3 + valences of Mn and Fe, and a small moment of less than 0.05 μ_B at Nb or Ta site. The rest of the moment was found at O sites owing to the finite covalency effect.

The dielectric, dielectric pulse, and ferroelectric (FE) hysteresis measurements show that Mn_2FeMO_6 (M = Nb, Ta) are insulating paraelectrics at low temperature and paraelectric plus conducting at high temperatures and room temperature (Supporting Information, Figures S9 and S10). There is neither a FE P(E) hysteresis loop in ferroelectric measurements nor a sharp, divergence-like anomaly in the dielectric permittivity (ε') observed, as expected for ferroelectric transitions. It is noteworthy that pyroelectricity was found in the samples at lower temperature, where the samples are not too conducting. Thus, the materials are polar and pyroelectric but not ferroelectric, as the structural polarity is not switchable by external fields. Considering the symmetry with point group 3*m* (*C*3*v*), the polar axis is along the *c* axis, the polarization, *P*, was estimated to be 32 and 23 $\mu C\,cm^{-2}$ for M = Nb, and Ta, respectively, from DFT calculations using the Berry phase formalism.[19a] Although DFT calculations are known to overestimate the value of polarization, this further indicates that Mn_2FeMO_6 are promising candidates for piezoelectric and pyroelectric as well as nonlinear optical materials.

In conclusion, novel $LiNbO_3$-type polar magnetic oxides prepared at high pressure have been extended to the perovskite-related multiple B-site $A_2BB'O_6$ system. The polar nature of the as-prepared $LiNbO_3$-type Mn_2FeMO_6 (M = Nb, Ta) is established by powder synchrotron X-ray and electron-diffraction analyses, as well as by second harmonic generation effect, and theoretical calculations. These discoveries are of major significance and open up a new path for novel polar and magnetic materials. The variety of cations and structural versatility of the cation arrangement at both A and B sites in $A_2BB'O_6$, for example in the $A_2B^{3+}B'^{5+}O_6$ and $A_2B^{2+}B'^{6+}O_6$ series (A^{2+}), or $A_2B^{2+}B'^{4+}O_6$ (A^{3+}) could yield a large number of polar oxides, where A is an unusually small cation, including Mg^{2+}, Mn^{2+}, Zn^{2+}, or Sc^{3+}, In^{3+}, and B′ is a d^0 ion, such as Nb^{5+}, Ta^{5+}, Mo^{6+}, W^{6+}, or Ti^{4+}. These materials could be polar, and potentially multiferroic, piezoelectric, pyroelectric, and second-order nonlinear optical materials, with important technological applications.

Experimental Section

For details of the experiments and calculations, see the Supporting Information. Further details on the crystal structure investigation may be obtained from the Fachinformationszentrum Karlsruhe, 76344 Eggenstein-Leopoldshafen, Germany (fax: (+49) 7247-808-666; e-mail: crysdata@fiz-karlsruhe.de), on quoting the depository numbers CSD-425981 and CSD-425982.

Received: April 4, 2013
Published online: June 28, 2013

Keywords: density functional calculations · high-pressure chemistry · $LiNbO_3$-type structure · Mn_2FeMo_6 · polar magnetic oxides

[1] a) K. M. Ok, E. O. Chi, P. S. Halasyamani, *Chem. Soc. Rev.* **2006**, *35*, 710–717; b) C. N. R. Rao, A. Sundaresan, R. Saha, *J. Phys. Chem. Lett.* **2012**, *3*, 2237–2246.

[2] M. D. Donakowski, R. Gautier, J. Yeon, D. T. Moore, J. C. Nino, P. S. Halasyamani, K. R. Poeppelmeier, *J. Am. Chem. Soc.* **2012**, *134*, 7679–7689.

[3] a) A. A. Belik, T. Furubayashi, H. Yusa, E. Takayama-Muromachi, *J. Am. Chem. Soc.* **2011**, *133*, 9405–9412; b) M. R. Li et al., *J. Am. Chem. Soc.* **2012**, *134*, 3737–3747 (see the Supporting Information).

[4] a) Y. Inaguma, M. Yoshida, T. Katsumata, *J. Am. Chem. Soc.* **2008**, *130*, 6704–6705; b) I. Yoshiyuki, Y. Masashi, T. Takeshi, A. Akihisa, T. Kie, K. Tetsuhiro, M. Daisuke, *J. Phys. Conf. Ser.* **2010**, *215*, 01231.

[5] A. A. Belik, T. Furubayashi, Y. Matsushita, M. Tanaka, S. Hishita, E. Takayama-Muromachi, *Angew. Chem.* **2009**, *121*, 6233–6236; *Angew. Chem. Int. Ed.* **2009**, *48*, 6117–6120.

[6] A. Aimi, T. Katsumata, D. Mori, D. FU, M. Itoh, T. Kyômen, K. Hiraki, T. Takahashi, Y. Inaguma, *Inorg. Chem.* **2011**, *50*, 6392–6398.

[7] T. Varga et al., *Phys. Rev. Lett.* **2009**, *103*, 047601 (see the Supporting Information).

[8] K. I. Kobayashi, T. Kimura, H. Sawada, K. Terakura, Y. Tokura, *Nature* **1998**, *395*, 677–680.

[9] G. V. Bazuev, B. G. Golovkin, N. V. Lukin, N. I. Kadyrova, Y. G. Zainulin, *J. Solid State Chem.* **1996**, *124*, 333–337.

[10] R. Mathieu, S. A. Ivanov, I. V. Solovyev, G. V. Bazuev, P. Anil Kumar, P. Lazor, P. Nordblad, *Phys. Rev. B* **2013**, *87*, 014408.
[11] D. Walker, M. A. Carpenter, C. M. Hitch, *Am. Mineral.* **1990**, *75*, 1020 – 1028.
[12] J. C. H. Z. Spencce, J. M. Zuo, *Electron Microdiffraction*, Plenum, New York, **1992**.
[13] J. Ko, C. Prewitt, *Phys. Chem. Miner.* **1988**, *15*, 355 – 362.
[14] N. Lliev, M. V. Abrashev, H. G. Lee, V. N. Popov, Y. Y. Sun, C. Thomsen, R. L. Meng, C. W. Chu, *J. Phys. Chem. Solids* **1998**, *59*, 1982 – 1984.
[15] M. W. Lufaso, R. B. Macquart, Y. Lee, T. Vogt, H.-C. zur Loye, *J. Phys. Condens. Matter* **2006**, *18*, 8761.
[16] E. J. Cussen, J. Vente, P. D. Battle, T. C. Gibb, *J. Mater. Chem.* **1997**, *7*, 459 – 463.
[17] L. Nathascia, S. Philippe, L. Alessandra Geddo, *J. Phys. Condens. Matter* **1999**, *11*, 3489.
[18] L. Nathascia, S. Philippe, L. Alessandra Geddo, *J. Phys. Condens. Matter* **2000**, *12*, 2367.
[19] a) J. P. Perdew, K. Burke, M. Ernzerhof, *Phys. Rev. Lett.* **1996**, *77*, 3865; b) V. I. Anisimov, J. Zaanen, O. K. Andersen, *Phys. Rev. B* **1991**, *44*, 943; c) G. Kresse, J. Hafner, *Phys. Rev. B* **1993**, *47*, 558; d) G. Kresse, D. Houbert, *Phys. Rev. B* **1999**, *59*, 1758.

